Steel-Plate Composite Wall-to-Reinforced Concrete Wall Mechanical Connection—Part 1: Out-of-Plane Flexural Strength

JUNGIL SEO, HASSAN S. ANWAR, AMIT H. VARMA, and YOONHO NAM

ABSTRACT

In safety-related nuclear structures, steel-plate composite (SC) walls are often used in combination with reinforced concrete (RC) walls or foundations. Appropriate connections are required to transfer force demands from the SC walls to the RC components without the connection failure that is often associated with brittle failure mode. This paper presents a design procedure developed for mechanical connections between SC and RC walls. This procedure implements the full-strength connection design approach in ANSI/AISC N690-18, *Specification for Safety-Related Steel Structures for Nuclear Facilities* (AISC, 2018), which requires connections to be stronger than the weaker of the connected walls. This paper also presents the results from experimental and analytical investigations conducted to verify the structural performance of the full-strength SC-to-RC connection. The focus of this paper (Part 1) is on the evaluation of the performance, strength, and ductility of SC wall-to-RC wall mechanical connections subjected to out-of-plane flexure. The results include global force-displacement responses, observations on concrete crack propagation, as well as applied force-strain responses of the connection region. The experimentally observed and analytically predicted results verify the conservatism of the proposed design procedure.

Keywords: steel-plate composite, reinforced concrete, mechanical connection, full-strength connection design, out-of-plane moment, LS-DYNA.

INTRODUCTION

A steel-plate composite (SC) wall is typically comprised of plain concrete reinforced with two steel faceplates, as shown in Figure 1. The faceplates are attached to concrete using shear connectors and connected to each other using tie bars. Shear connectors provide composite action, whereas tie bars provide structural integrity and serve as out-of-plane reinforcement. Significant experimental and analytical research has been conducted around the world on the behavior and design of SC walls over the last two decades for various force demands including in-plane shear (Ozaki et al., 2004; Lee et al., 2009; Song et al., 2014; Bhardwaj et al., 2019), out-of-plane flexure and shear (McKinley and Boswell, 2002; Foundoukos and Chapman, 2008; Hong et al., 2009; Leng et al., 2015; Sener et al., 2015), axial compression (Takeuchi et al., 1998; Choi and Han, 2009; Zhang et al., 2020), and impact loading (Bruhl et al., 2015a; Kim et al., 2020). The results from some of the aforementioned and other research programs have been used to develop design specifications and aids such as JEAC-4618 (JEAC, 2009), KEPIC-SNG (KEA, 2010), AISC N690 (AISC, 2018), AISC Design Guide 32 (Bhardwaj and Varma, 2017), and AISC 341-16 (AISC, 2016).

Previously conducted research has proven that SC walls have superior structural performance over conventional RC walls. In addition, the recent construction of SC walls for nuclear power plants (AP1000® nuclear power plants in China and Vogtle, Georgia) and a high-rise building in Seattle (Rainier Square, utilizing composite steel-plate shear wall systems) have proven that SC walls can reduce the overall construction duration. For these reasons, SC walls are continuously gaining interest from both (1) the nuclear industry for the third generation of nuclear power plants as well as small modular reactors (SMRs) and (2) the building industry for the application to core wall of high-rise structures.

Despite their advantages and potential as an alternative to conventional reinforced concrete (RC) described earlier, it is challenging to completely replace RC structures with SC walls in an entire structure due to relatively higher material and fabrication costs as well as the designer's personal preference to use RC walls for certain applications. Therefore, there is an inevitable need for providing joints between SC walls and RC structural elements. SC

Jungil Seo, Research Assistant Professor, Purdue University, West Lafayette, Ind. Email: seo2@purdue.edu (corresponding)

Hassan S. Anwar, Graduate Research Assistant, Purdue University, West Lafayette, Ind. Email: hsagheer@purdue.edu

Amit H. Varma, Karl H. Kettelhut Professor and Director of Bowen Laboratory, Purdue University, West Lafayette, Ind. Email: ahvarma@purdue.edu

Yoonho Nam, Engineering Group Supervisor, Civil & Architectural Engineering Department, KEPCO E&C, Korea, yoonho.nam@gmail.com

Paper No. 2021-01

wall-to-RC connections can be found when (1) SC walls are connected to RC floor slabs, (2) SC walls are connected to an RC basemat, and (3) SC walls are connected to RC walls. Only the SC wall-to-RC wall connection is considered in this study because the other two connections have already been previously investigated both experimentally and analytically (Kurt, 2016; Seo and Varma, 2017c).

The design demands need to be transferred properly from one structure to the other structure through the connection region so that the maximum benefits of SC walls can be achieved. Connecting SC and RC walls can be achieved using noncontact lap splice or mechanical connections. Multiple curtains of large reinforcement (in diameter) are typically placed for RC walls subjected to higher design demands. Connecting SC walls to RC walls using the noncontact lap splicing for reinforcement bars larger than 1.4-in. diameter (#11) would require a significantly longer development length, which may not be suitable for some locations. To overcome this challenge, mechanical connection of reinforcement bars greater than 1.4-in. diameter (#11) can be considered as per ACI 349-06 (ACI, 2006).

Although ACI 349-06 (ACI, 2006) specifies the design requirements for mechanical connection of reinforcement bars in RC construction, it cannot be easily extended to SC wall-to-RC wall mechanical connections due to complex force transfer mechanisms associated with two different structural systems and lack of detailed design requirements in ANSI/AISC N690-18, *Specification for Safety-Related Steel Structures for Nuclear Facilities* (AISC, 2018), hereafter referred to as AISC N690. For these reasons, a design procedure for SC-RC mechanical connections was developed by the authors based on available and existing connection design philosophy and concepts. The procedure was evaluated experimentally and analytically, and this paper focuses on the experimental and analytical investigation of the SC-RC mechanical connections subjected to out-of-plane flexure. It presents (1) the development of the design procedure, (2) results and observations from both experimental and analytical investigation, and (3) the validity of the design procedure.

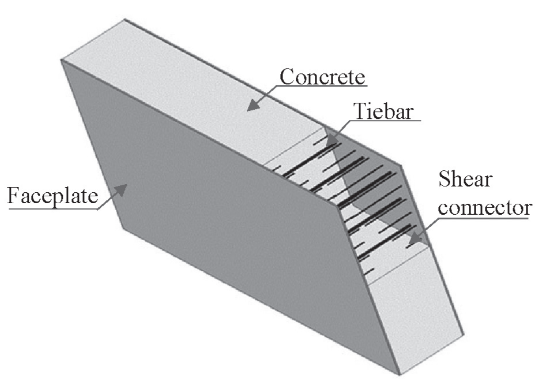

Fig. 1. Typical SC wall configuration.

BACKGROUND

The typical SC wall connections to RC structures include (1) SC wall-to-RC slab, (2) SC wall-to-RC foundation, and (3) SC wall-to-RC wall. These SC wall connections can be designed based on two different connection design philosophies for SC wall connections permitted by AISC N690 (AISC, 2018), and they use both full-strength connection design philosophy and overstrength connection design philosophy. With the full-strength connection implemented, the connection is strong enough to develop the full strength (125%) of the weaker of the connected structural components. It is often associated with forming plastic hinges away from the connection region, dissipating energy during design basis seismic events. Thus, the connection philosophy is often recommended and preferred. On the other hand, with the overstrength connection implemented, the connection can be weaker than the connected structural components, but its strength is designed to be greater than or equal to 200% of the seismic demands and +100% of the nonseismic demands in the load combination.

Seo and Varma (2017b, 2019) conducted experimental and analytical investigations for SC wall-to-wall connections (T and L joints). The focus was on understanding the behavior of SC wall joints and developing design recommendations. The authors developed a connection design method for SC wall-to-wall T and L joints by implementing a full-strength connection design philosophy and recommended a design equation for the strength of SC wall joints. However, SC wall-to-RC structure connections can be difficult to design due to a complex force transfer mechanism and the absence of specific design aids and specifications.

JEAC (2009) recommends three connection techniques to transfer the forces from SC wall to RC foundation: noncontact lap splicing between foundation dowel bars and SC wall steel faceplates [technique (a)], steel faceplates of SC wall embedded into the RC foundation using shear studs [technique (b)], and steel faceplates and embedded foundation dowel bars welded to the baseplate [technique (c)]. These three techniques are shown in Figure 2. Connection techniques (a) and (c) were experimentally and analytically investigated by Kurt (2016). A total of 10 tests were conducted with aspect ratios (height/length of SC wall) from 0.60 to 1.00. The specimens were subjected to cyclic in-plane loading, and the failure of the specimens occurred as crushing of concrete and fracture of steel dowel bars. The SC wall-to-RC foundation anchorage connection technique (a) subjected to monotonic tension loading was investigated by Seo and Varma (2017a). Three full-scale specimens were designed based on a full-strength connection design philosophy. The focus was on the influence of shear reinforcement, dowel embedment length, and tie bar configuration on the axial behavior and force transfer mechanism of the SC-to-RC lap splice connection. Based on the results from this study, the authors concluded that the ductile behavior of the SC-to-RC lap splice connection can be led by developing concrete compressive struts within the connection

Researchers including Hwang et al. (2013), and Lee et al. (2012) have discussed the behavior of the SC wall-to-RC wall (L-joint) connection. For example, Hwang et al. carried out an experimental and analytical study to evaluate the strength, ductility, and failure mode of the noncontact lap splice (L-joint) connection, shown in Figure 3. The L joint exhibited ductile failure mode with yielding of vertical reinforcement in the connection region governing the overall force-displacement behavior. Additionally, Lee et al. carried out a similar experimental program and reported flexural reinforcement pull out along with RC wall shear failure.

DESIGN PROCEDURE

RC or SC walls in any structure are designed for seismic and nonseismic load combinations resulting in design demands. These design demands are transferred from one wall to the other through the connection region. Although AISC N690 (AISC, 2018) recommends two connection design philosophies (full-strength and overstrength), it does not provide a detailed design approach and recommendations for SC

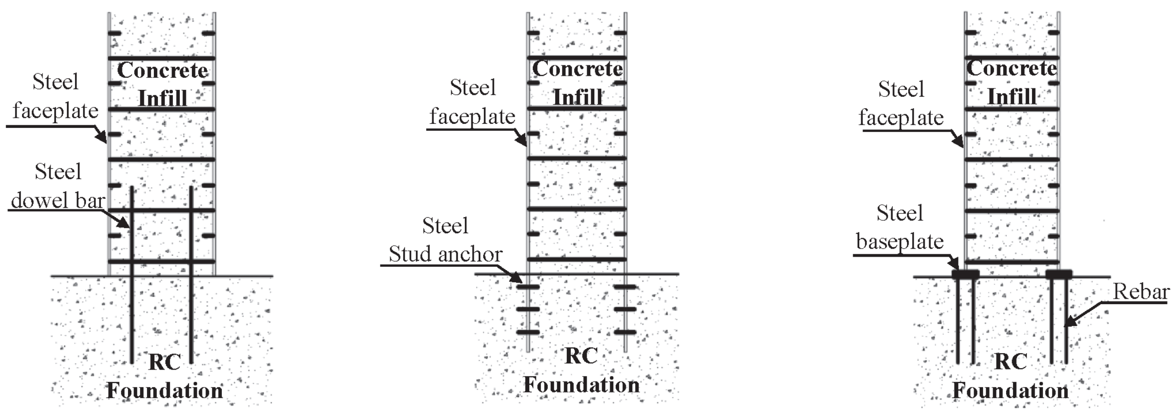

(a) Noncontact lap splicing *(b) Embedding* *(c) Anchoring*

Fig. 2. Connection techniques for SC wall-to-RC foundation (Seo and Varma, 2017a).

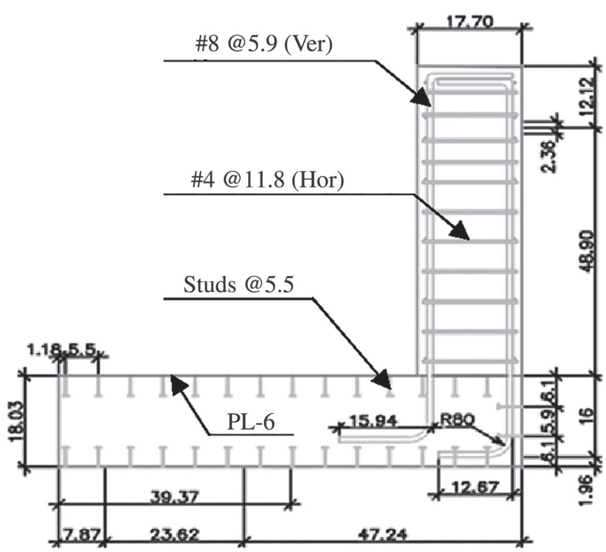

Fig. 3. SC wall-to-RC wall noncontact lap splice (L-joint) connection (units: in.) (Hwang et al., 2013).

wall-to-RC wall mechanical connections. In addition, there are no SC wall-to-RC wall mechanical connections that have been previously developed and tested. The authors have developed a design procedure for SC wall-to-RC wall mechanical connections based on the full-strength connection design philosophy.

When SC walls are implemented and connected to RC walls, these design demands must be transferred to connected structural components. Figure 4 illustrates four major design force demands on an RC wall panel section near the SC wall-to-RC wall connection, including axial tension (S_x, S_y), in-plane shear force (S_{xy}, S_{yx}), out-of-plane shear force (S_{xz}, S_{yz}), and out-of-plane flexural or twisting terms (M_x, M_y, M_{xy}, M_{yx}). In general, M_{xy} and M_{yx} are obtained from finite element analysis and added to M_x and M_y, respectively. In addition, S_x, S_{xy}, S_{xz}, and M_x are resisted by the RC and SC walls independently; therefore, these terms are not required to be transferred to the SC wall. Thus, only four force terms (S_y, S_{yx}, S_{yz}, M_y), shown in Figure 5, need to be transferred from RC wall to SC wall. S_y is the axial force in the y-direction (T) and M_y is the out-of-plane moment (OOPM). S_{yx} and S_{yz} are the in-plane shear (IPV) and the out-of-plane shear (OOPV), respectively.

Figure 6 presents a schematic view of a typical SC wall-to-RC wall mechanical connection considered in this study. As shown, reinforcement embedded in the RC wall is extended and connected to the baseplate using mechanical couplers. The baseplates are welded to the faceplates and the wing plates to resist the force from the rebars. The steel tie plates are placed and welded to the faceplates to provide the resistance against the tension force induced by the moment generated from the eccentricity.

Figure 7 illustrates the axial force, T, transfer through the mechanical connection from the RC wall to the SC wall. As shown, the rebar in the RC wall are extended and connected to the baseplate that is welded to both the wing plate and the faceplate of the mechanical connection. With the full-strength connection design philosophy, the maximum axial force that needs to be transferred to the SC wall is 125% of the yield strength of the reinforcing bars ($T_1 = T_2 = T_3 = T_4 = 1.25A_{s,r}F_{y,r}$). This maximum axial force is referred to as the required axial tension strength, N_r, and it is equally distributed between the two faceplates. The required axial tension strength, N_r, in the rebars is transferred to the faceplates and generates the moment due to the eccentricity. The moment is resisted by concrete in compression and the tie plate in tension that connects the two faceplates.

Figure 8 illustrates the out-of-plane moment (OOPM) transfer mechanism from the RC wall to the SC wall. As shown, the OOPM is transferred to the SC wall through compression force in the concrete and tension force in the steel rebar and the faceplates. The maximum OOPM that needs to be transferred through the mechanical connection is 125% of the flexural strength of the RC wall,

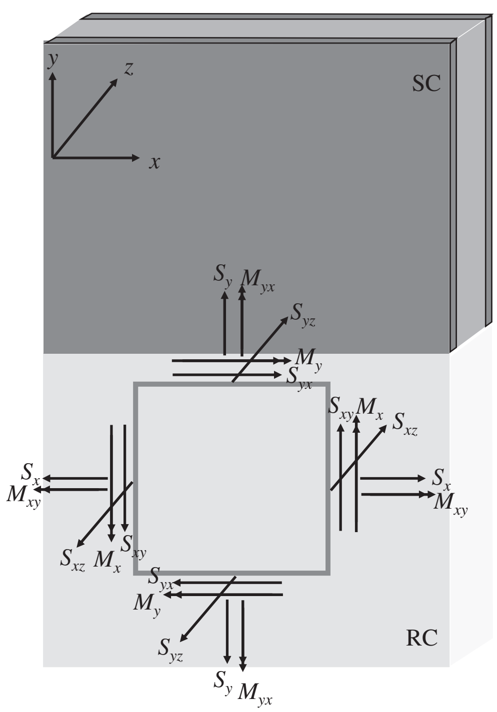

Fig. 4. Forces on RC wall panel section.

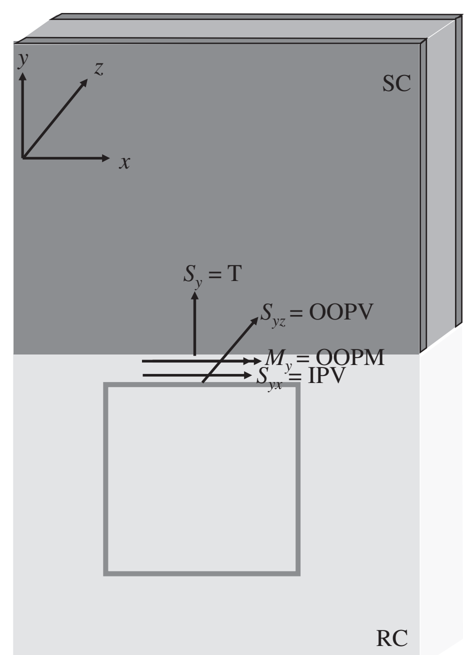

Fig. 5. Four forces on RC wall panel to be transferred to SC wall.

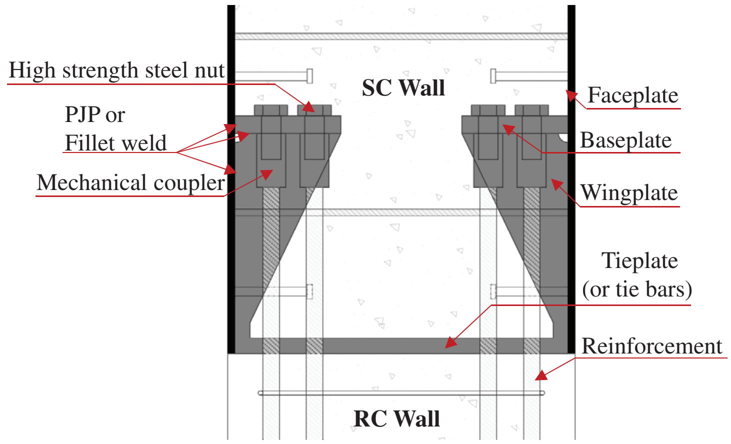

Fig. 6. Schematic of the mechanical splice connection.

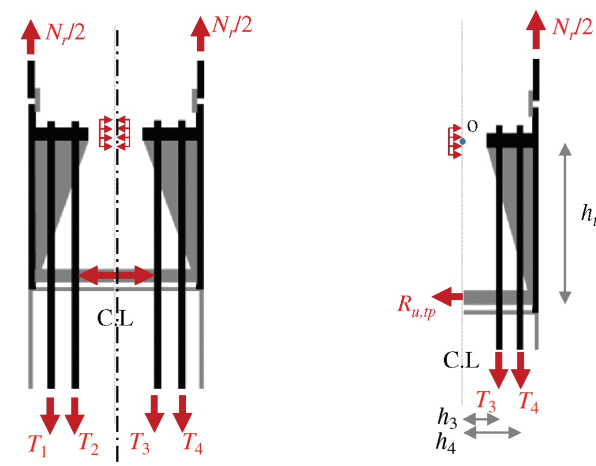

Fig. 7. Axial force transfer mechanism.

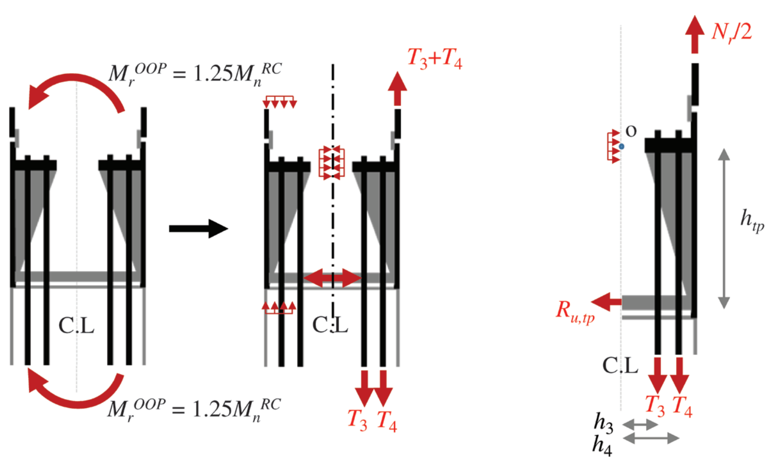

Fig. 8. Out-of-plane moment force transfer mechanism.

M_n^{RC}. Thus, the required OOPM, M_r^{OOP}, is $1.25M_n^{RC}$. The M_r^{OOP} also generates an eccentric moment, and it is resisted by the SC wall infill concrete in compression near the baseplate, and the tensile force in the tie plate that connects the two faceplates.

For both the out-of-plane shear (OOPV) and the in-plane shear (IPV), the shear friction is the main force transfer mechanism, as shown in Figure 9. When the mechanical splice connection is subjected to either of the two shear forces, the shear transfer occurs across two planes via friction between the two concrete surfaces. The friction force is a result of the clamping forces created by the rebar keeping the two surfaces together. The maximum transferred shear force between two concrete surfaces, V_n^{SF}, is limited by the lesser of $0.2f_c'A_c$, $1600A_c$, or $(480 + 0.08f_c')A_c$ according to ACI 318-19, Section 22.9.4.4 (ACI, 2019), where A_c is the area of concrete resisting shear transfer.

In general, the out-of-plane shear strength of RC walls is less than the shear friction force. Thus, the mechanical splice connection will not fail prior to the shear failure of the RC wall as long as the connection region can transfer the shear friction force. For this reason, the mechanical connection is designed based on the assumption that all the rebars connected to the connection develop 125% of their yield strength, which results in the moment due to the eccentricity induced by the required axial tension strength, N_r. Similarly, the moment is resisted by concrete near the baseplate and the tie plate that connects the two faceplates.

The design procedure developed in this study in underlying sections assumes that (1) both RC and SC walls have been designed, (2) wall thickness of the RC wall is the same as the wall thickness of the SC wall, and (3) width of the baseplate is the same as the maximum width of the wing plate. The procedure can be generalized in three steps: (1) tie plate design, (2) baseplate design, and (3) wing plate design.

Tie Plate (TP) Design

Designing the steel tie plate involves identifying the required axial tension force for the tie plate, $R_{u,tp}$. As shown in Figures 7 and 8, the magnitude of $R_{u,tp}$ is influenced by the distance of the tie plate with respect to the baseplate, h_{tp}, and the rebar distance, h_3 and h_4, with respect to the section centerline (CL). From the free-body diagrams, $R_{u,tp}$ can be calculated by taking a moment at location O, as given in Equation 1. In the equation, N_r is the sum of T_1, T_2, T_3, and T_4. T_1, T_2, T_3, and T_4 are the respective full strengths of the steel rebar $(1.25A_{s,r}F_{y,r})$. In addition, t_{wall} is the wall thickness, and t_p is the faceplate thickness.

$$R_{u,tp} = \frac{\left[\frac{N_r}{2}\left(\frac{t_{wall}}{2} - \frac{t_p}{2}\right)\right] - (T_3h_3 + T_4h_4)}{h_{tp}} \tag{1}$$

Baseplate Design

The baseplate design can be performed using the yield line method. The yield line method is based on the bending moment of the structural element at its collapse state. The unit baseplate is subjected to two concentrated forces, equal

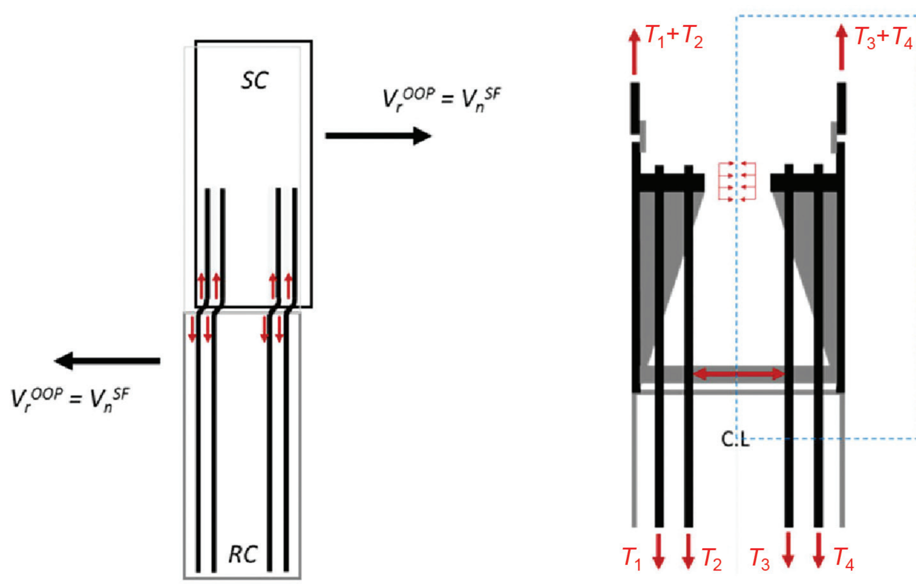

Fig. 9. Out-of-plane shear and in-plane shear force transfer mechanism.

to 125% of the yield strength of the steel rebar, $1.25A_{s,r}F_{y,r}$. As shown in Figure 10, the three perimeters of the unit baseplate reach their negative flexural strength, M_{bp}^{-}, forming yield lines l_4, l_5, and l_6. Three additional yield lines, l_1, l_2, and l_3, (as a result of positive flexural strength, M_{bp}^{+}, are formed inside the unit baseplate connecting the concentrated forces, P, the bottom center point, and the two top corners, respectively. The spacing and thickness of the wing plate are S_{wp} and $t_{p,wp}$, respectively. In addition, W_{wp} is the width of the wing plate, S_{r1} is the distance of the rebar to the faceplate, and S_{r2} is the center-to-center distance between rebar. With the yield line analysis method, it is assumed that the work done by external forces, $\sum W_{ext}$, in undergoing a small deflection, Δ, is equal to the internal work, $\sum W_{int}$, done in rotations along yield lines, θ_1 and θ_2; see Figure 11. Equating $\sum W_{ext}$ and $\sum W_{int}$ will result in the required flexural strength of the baseplate, $M_{u,bp}$, per unit length (1 in.). The external and internal work, $\sum W_{ext}$ and $\sum W_{int}$, are given in Equations 2 and 3, and the required flexural strength, $M_{u,bp}$, is given in Equation 4.

$$\sum W_{ext} = 2P\Delta = 2(1.25A_{s,r}F_{y,r})\Delta \tag{2}$$

$$\sum W_{int} = \sum(Ml\theta) \tag{3}$$

$$M_{u,bp} = M = \frac{2(1.25A_{s,r}F_{y,r})\Delta}{2l_1\theta_1 + l_2(\theta_1+\theta_2) + l_3(\theta_1+\theta_2) + l_4\theta_1 + l_6\theta_1 + l_5\theta_2} \tag{4}$$

where

$$l_1 = W_{bp} - S_{r1} - 1.5d_{hole}$$

$$l_2 = l_3 = \sqrt{\left(\frac{S_{wp} - t_{p,wp}}{2}\right)^2 + (S_{r1})^2} - \frac{1}{2}d_{hole}$$

$$l_4 = l_6 = W_{bp}$$

$$l_5 = S_{wp} - t_{p,wp}$$

$$\Delta = 1$$

The minimum baseplate thickness can be calculated by equating $M_{u,bp}$ and $\phi M_{n,bp}$ (i.e., $\phi M_{n,bp} = \phi F_y Z$) using Equation 5.

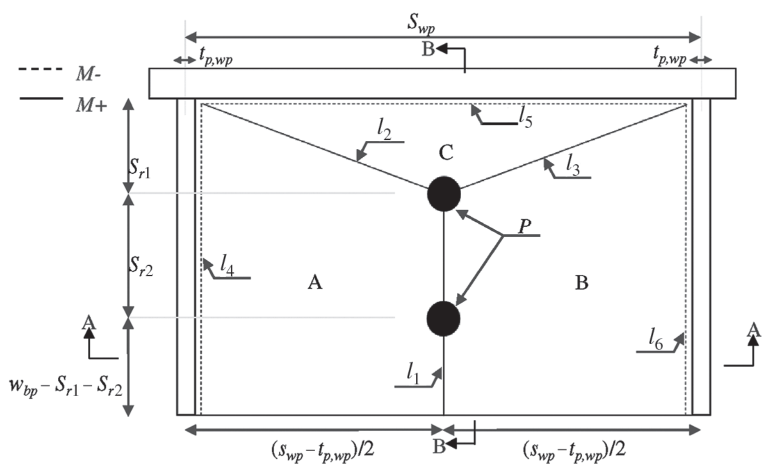

Fig. 10. Yield lines for unit baseplate.

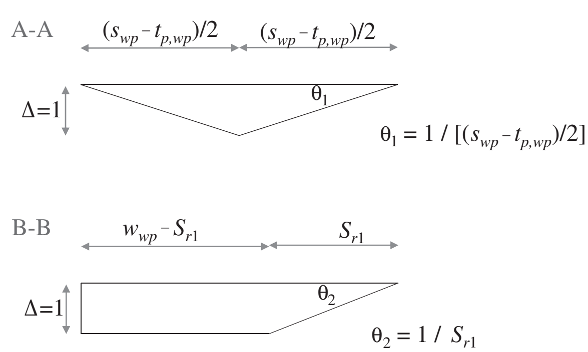

Fig. 11. Small deflection angles at section A-A and B-B.

$$t_{p,bp,min} = \sqrt{\frac{8(1.25A_{s,r}F_{y,r})}{\frac{2l_2\theta_1 + l_2(\theta_1+\theta_2) + l_3(\theta_1+\theta_2) + l_4\theta_1 + l_6\theta_1 + l_5\theta_2}{\phi F_{y,bp}}}} \tag{5}$$

where

$$Z = \frac{(1\text{ in.})(t_{p,bp})^2}{4}$$

Wing Plate Design

In this design process, the thickness of the wing plate is determined. Figure 12 illustrates a single wing plate that is subjected to axial compression force from four reinforcing bars located on both sides of the wing plate. As shown, the geometry of the system, as well as the loading condition, is similar to those of the triangular bracket seat in AISC *Companion to the AISC Steel Construction Manual, Volume 1: Design Examples* (AISC, 2019). Thus, the design process for the triangular bracket seat can be implemented for the steel wing plate if the variables P, a, and b as shown in Figure 12(b) are replaced with $T_1 + T_2$, h_{tp}, and W_{bp}, as shown in Figure 12(a), respectively. During the wing plate design process, demands and available strengths at sections A-A and B-B are calculated and compared.

EXPERIMENTAL INVESTIGATION

The design procedure developed for SC wall-to-RC wall mechanical connections was verified experimentally. A total of seven tests (four full scale and three small scale) were conducted to evaluate the performance of the SC wall-to-RC mechanical connections designed through the procedure. They were subjected to monotonic OOPM and OOPV and cyclic in-plane shear (IPV). In this paper, only two large specimens subjected to OOPM are discussed. The results from the remaining five specimens subjected to OOPV and IPV will be published later.

Design of Test Matrix

The specimens were designed to depict a unit cell of a typical wall section in nuclear facilities. The typical configuration of the test specimens is shown in Figure 13. As shown, the specimens had a wall thickness, T_{wall}, and width, w_{wall}, of 36 in., with a span length, l_{span}, of 324 in. ($9.0T_{wall}$). The RC wall portion had flexural reinforcement placed in four curtains, a pair along each edge, comprised of ASTM A706 (ASTM, 2016) Grade 60 #14 rebar at center-to-center spacing, $s_{1,rc}$, of 9 in., with a longitudinal reinforcement ratio, ρ_1, of 0.027. Shear reinforcement was comprised of ASTM A706 Grade 60 #4 double hoop stirrups at the same center-to-center spacing of 9 in. along the length of the wall. The SC wall portion of the test specimens consisted of ¾-in.-thick, Grade 50 faceplates, resulting in a reinforcement ratio, ρ_2, of 0.04; 1-in.-diameter stud anchors at center-to-center spacing, s_s, of 9 in.; and ASTM A706 Grade 60 #8 tie bars welded with a partial-joint-penetration groove weld to faceplates at a center-to-center spacing, s_t, of 18 in. The mechanical connection region was designed using the proposed design procedure. The 27-in.-long connection region was comprised of a 2-in.-thick (t_{bp}) and 11-in.-wide baseplate (w_{bp}), 1-in.-thick wing plate (t_{wp}), and a 1-in.-thick (t_{tp}) and 1¾-in.-wide tie plate (w_{tp}). All steel plates within the mechanical connection region were Grade 50.

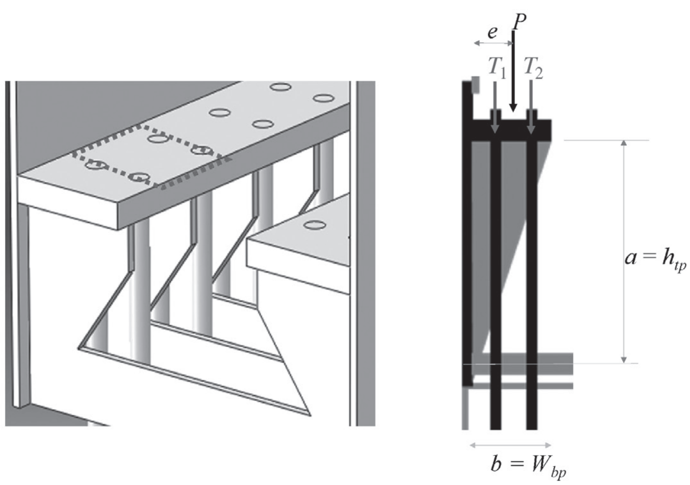

(a) Wing plate

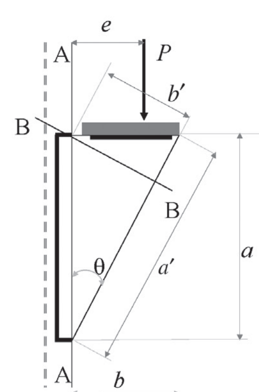

(b) Bracket seat design per AISC (2019)

Fig. 12. Design comparison.

Table 1 presents geometric details of the test specimens. The two specimens in Table 1 are essentially identical specimens. They are only differentiated by their names as well as longitudinal rebar-to-baseplate connection plans. Figure 14 illustrates the two rebar-to-baseplate connection plans considered in this study. The coupler plan shown in Figure 14(a) utilizes a coupler that connects with the tapered threaded #14 reinforcing bar at one end. The coupler is then bolted to the baseplate using ASTM A449 (ASTM, 2020) high-strength bolts. The bolt is stronger than the connected reinforcing bar with a tensile strength, F_u, of 90 ksi and required no special tightening considerations. Similarly, the double nut plan as shown in Figure 14(b) also utilizes the tapered threaded #14 reinforcing bar, which is connected to the baseplate using the coupler and a threaded rod.

The steel components of the two specimens were made from the same heat. The steel material properties were measured by conducting uniaxial tension tests according to ASTM E8 (ASTM, 2013). Table 2 summarizes the average measured steel material properties of the test specimens used in the study. In Table 2, F_y is the average measured 0.2% offset yield stress. The concrete material properties were measured by conducting uniaxial compression tests according to ASTM C39 (ASTM, 2014) on 4-in.-diameter concrete cylinders that were cast at the same time as the test specimens. The average measured concrete strengths at day of test for the test specimens are also presented in Table 2.

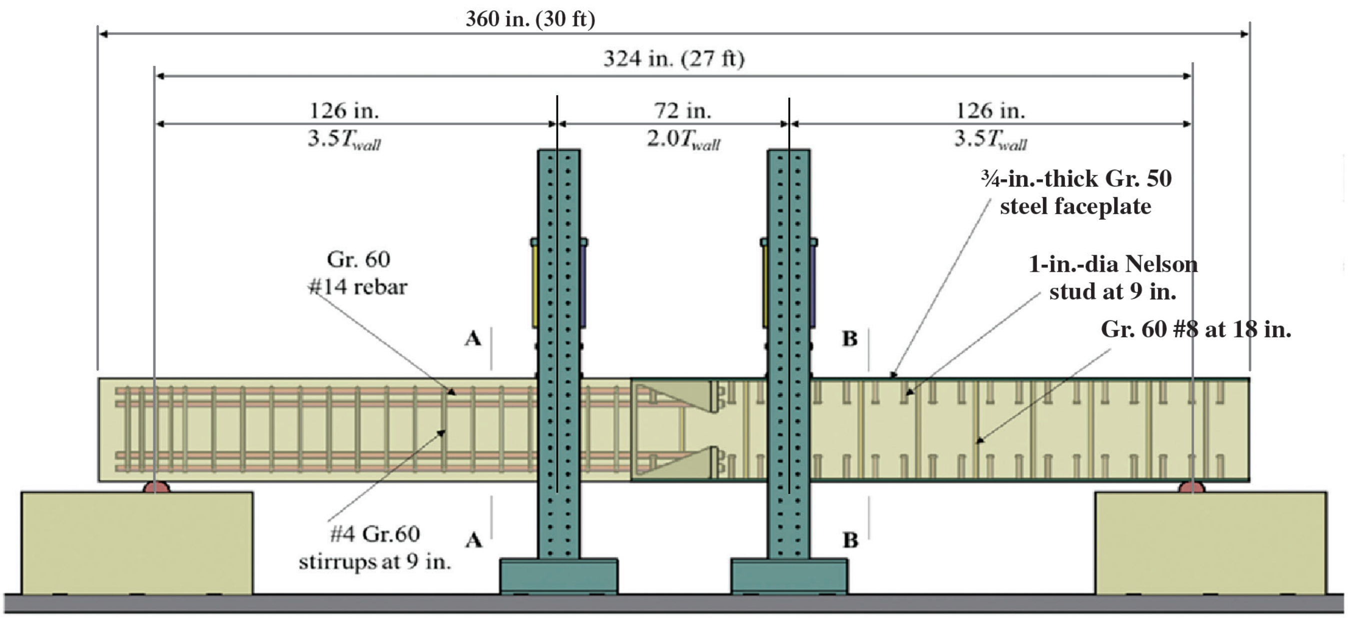

(a) Elevation view

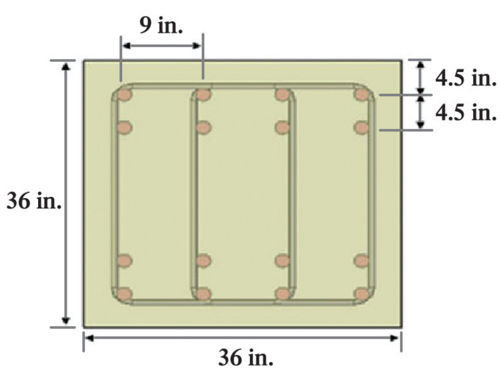

(b) Section view A-A

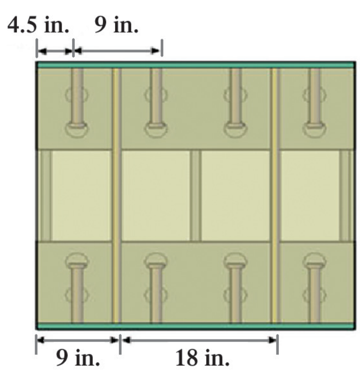

(c) Section view B-B

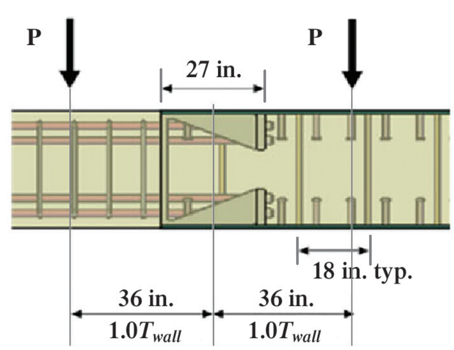

(d) Connection region

Fig. 13. OOPM test specimen.

Table 1. Geometric Details of OOPM Test Specimens															
Specimen	Overall Dimension			SC Wall				RC Wall			Connection				
	w_{wall} (in.)	l_{span} (in.)	T_{wall} (in.)	t_p (in.)	ρ_2	s_s (in.)	s_t (in.)	Rebar Size	$s_{1,rc}$ (in.)	ρ_1	w_{tp} (in.)	t_{tp} (in.)	w_{bp} (in.)	t_{bp} (in.)	t_{wp} (in.)
OOPM-C	36	324	36	¾	0.04	9	18	14	9	0.027	1.75	1	11	2	1
OOPM-DN	36	324	36	¾	0.04	9	18	14	9	0.027	1.75	1	11	2	1

Table 2. Measured Properties of OOPM Test Specimens							
Specimen	Steel Yield Strength, F_y, ksi						Concrete Strength, f'_c, psi
	Faceplate	Baseplate	Tie Plate	Wing Plate	Rebar	Stirrup	
OOPM-C	60	62	57	57	68	67	5,447
OOPM-DN	60	62	57	57	68	67	5,470

Instrumentation Plan

The OOPM test specimens were subjected to monotonic loading in the vertical direction, as illustrated in Figure 13. Two 500-kip hydraulic actuators were connected to the test frames to apply the monotonic loading at two locations 36 in. away from the center of the specimen.

The layout of string potentiometers (SPs) and displacement transducers (DTs) is illustrated in Figure 15. One set of two SPs were attached to the center of connection region to measure global deflection and possible twisting of the specimen. Another pair of SPs were attached to the bottom of the specimen under each loading point. Two DTs were placed under each roller support to measure support settlement. Four electrical-resistance strain gauges (SGs), each on the interior wing plates and tie plates, were attached as per the configuration shown in Figure 16. In case of baseplates, two SGs were attached, each on top and bottom baseplates at horizontal distances of 13.5 in. and 22.5 in., respectively, from the left face, as shown in Figure 17. Two SGs were attached on each #14 horizontal rebar (one at the top and one at the bottom of rebar) located at a horizontal distance of 2 in. from the mechanical coupler, making a total of 16 SGs in the specimen rebar cross section (connection region). This arrangement is illustrated in Figure 18.

EXPERIMENTAL OBSERVATIONS AND RESULTS

Specimen OOPM-C

The applied force–displacement response of specimen OOPM-C is shown in Figure 19. As shown, the first concrete flexural cracks occurred in the RC wall portion at the applied force of P = 80 kips, resulting in a change in the stiffness. Additionally, a significant decrease in the stiffness at P = 500 kips was observed due to yielding of the bottom #14 reinforcing bars. Concrete crushing under the loading point in the RC portion was also observed at P = 514 kips. The maximum applied force, P_{max}, was 585 kips, and the corresponding displacements were 6.39 in., 6.07 in., and 4.83 in. at the RC portion, center, and the SC wall portion, respectively. As expected, the maximum displacement, Δ_{max}, was observed in the RC wall portion of the specimen (SP4). The maximum applied force, P_{max}, was greater than the force associated with the flexural strength of the RC portion calculated using ACI 349 (ACI, 2006) provisions with the measured properties ($P_{Mn.RC}$ = 495 kips) by 18%. The shear force associated with P_{max} was 293 kips ($P_{max}/2$), less than the shear strength of the RC wall portion determined using ACI 349 ($V_{n.RC}$ = 329 kips), thus confirming

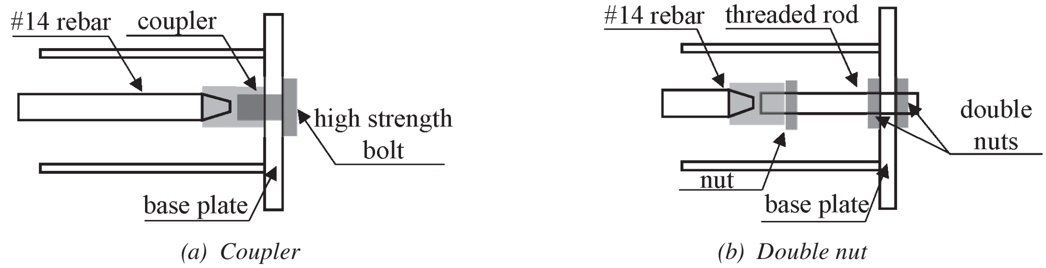

Fig. 14. Rebar to baseplate connections.

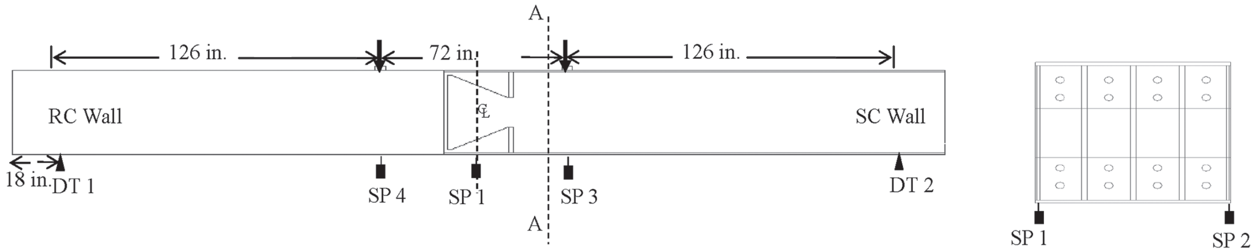

(a) Elevation view (b) Section view A-A

Fig. 15. SP and DT sensor layout.

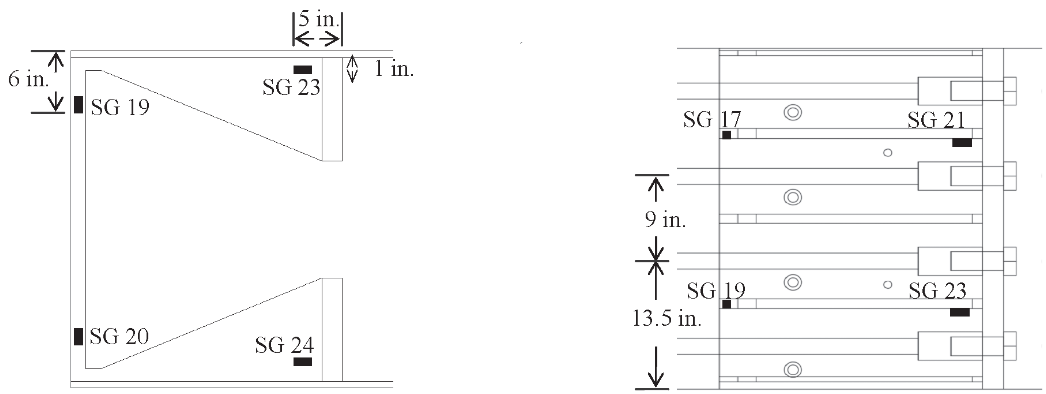

(a) Elevation view (b) Plan view

Fig. 16. SG layout of wing plates and tie plates.

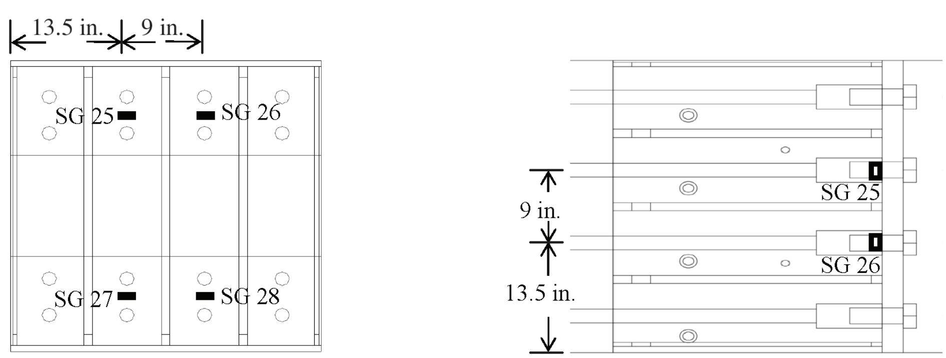

(a) Elevation view (b) Plan view

Fig. 17. SG layout of baseplates.

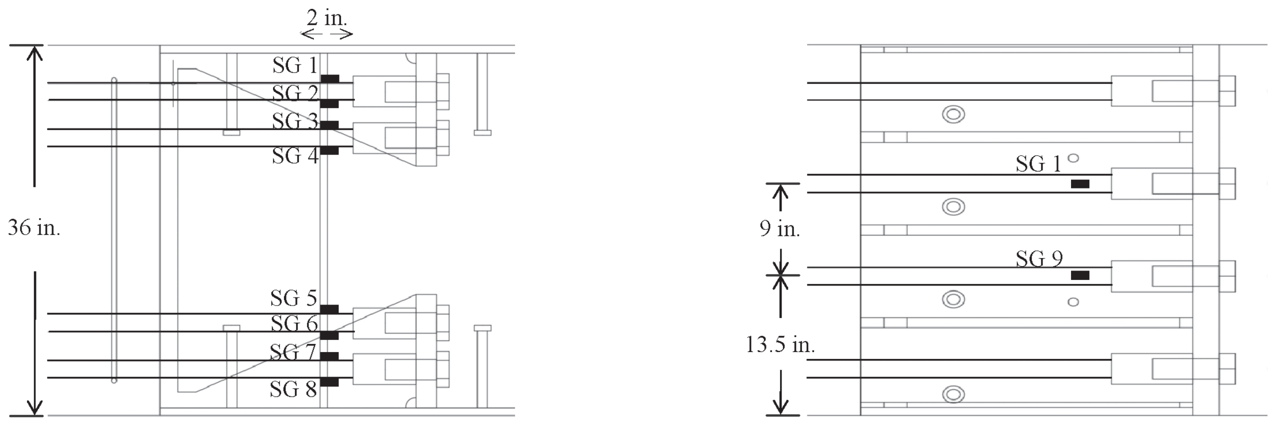

(a) Elevation view

(b) Plan view

Fig. 18. SG layout for #14 rebar.

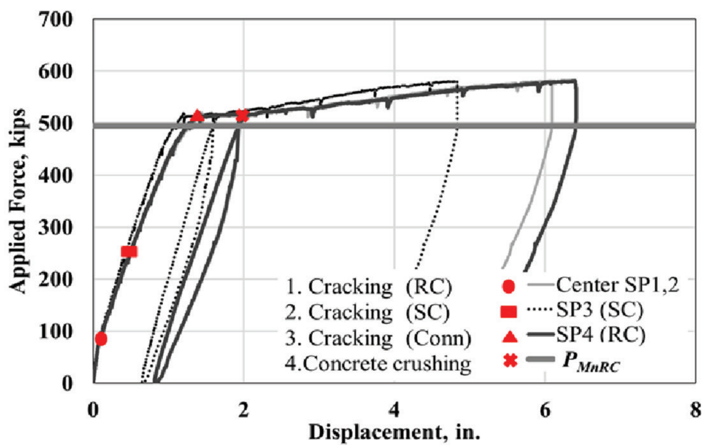

Fig. 19. Applied force–displacement response.

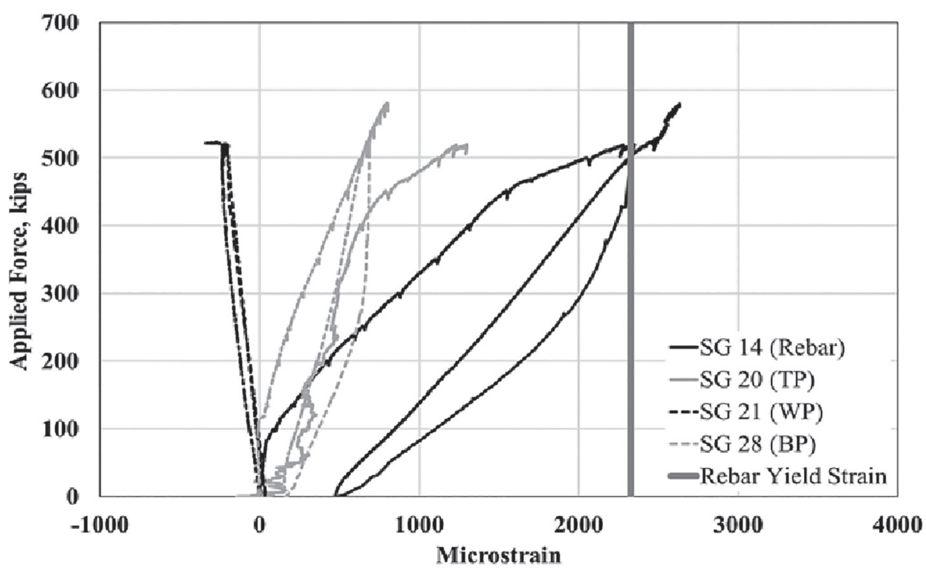

Fig. 20. Applied force–strain response of specimen OOPM-C (#14 rebar, wing plates, tie plates, and baseplates).

flexural yielding of the RC wall portion to be the governing failure mode.

Figure 20 shows the applied force–strain response for #14 rebar, wing plate, tie plate, and baseplate. The bottom #14 rebar exhibited the maximum strain of 2,640 με (SG 14), which was greater than the yield strain (ε_y = 2,330 με). Note that the maximum strain of the #14 rebar is somewhat lower than expected because the strain gauges were attached 2 in. away from the mechanical couplers rather than being attached at the interface between the RC wall and SC wall portions. As shown, the maximum strain for wing plates and tie plates at P_{max} was 1,440 με (SG 20, tie plate) and −360 με (SG 21, wing-plate), respectively, with corresponding stress values of 41.6 ksi and −10 ksi. Lastly, a similar response of baseplates is shown in the same figure exhibiting the maximum strain of 802 με (SG 28) at P_{max}. As expected, all steel components in the connection region remained in the elastic range.

Figure 21 presents the overall damage progression in terms of concrete crack patterns. First flexural cracks appeared in the bottom of RC wall portion near the loading point at 14% of P_{max}. As the loading increased, additional flexural cracks were formed within the RC wall shear span as well as in the SC wall region around 235 kips ($0.4P_{max}$). The flexural cracks transformed into flexural-shear cracks at $0.6P_{max}$. Cracks appeared in the connection region just before the onset of concrete crushing at the RC wall portion loading point. After the yielding of the #14 rebar, the compression zone under the loading point (RC wall portion) softened as a result of concrete crushing and spalling, causing extensive ductile deformation of the test specimen, as shown Figure 22.

Specimen OOPM-DN

Figure 23 shows the applied force–displacement response of specimen OOPM-DN. As shown in the figure, the specimen exhibited similar behavior to that of OOPM-C. The maximum applied load was P_{max} = 570.8 kips, and the corresponding displacements were 4.98 in., 4.80 in., and 3.79 in. at the RC portion, center, and the SC wall portion, respectively. The maximum vertical displacement, Δ_{max},

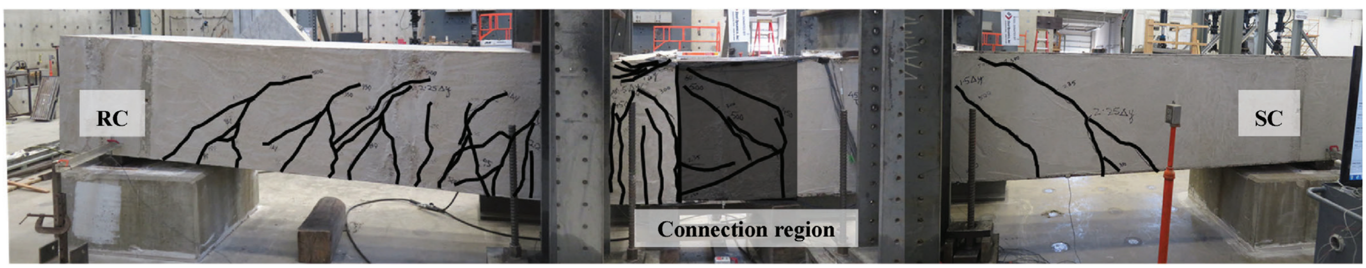

Fig. 21. Concrete crack pattern (east side)—specimen OOPM-C.

(a) Gap opening at the RC-SC interface

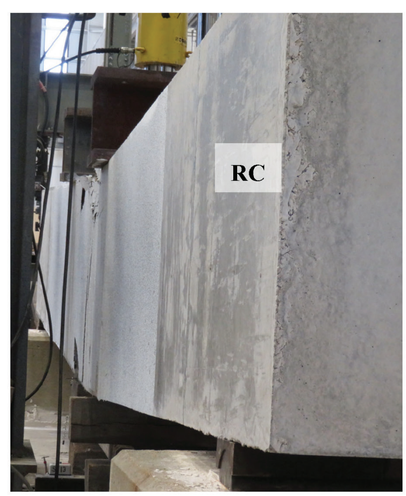

(b) Significantly deformed specimen

Fig. 22. Damage of specimen OOPM-C.

was measured from the RC wall portion of the specimen (SP4). P_{max} was greater than the force associated with the flexural strength of the RC wall portion calculated using ACI 349 (ACI, 2006) provisions ($P_{Mn.RC}$) with the measured material properties by 75.8 kips (15%).

Figure 24 shows the applied force-strain response of the #14 rebar. The bottom #14 rebar exhibited strain values greater than their yield strain (ε_y = 2,330 με) at P_{max}, with maximum strain value of 2,710 με (SG 8). The same figure presents the response of wing plates and tie plates. The plates remained in the elastic range during the test, exhibiting maximum strain of 1,670 με (tie plates, SG 20) and −297 με (wing plates, SG 23) at P_{max}, respectively. The applied force-baseplate strain response shows the maximum strain of 176 με (SG 27).

Figure 25 shows the overall damage progression in terms of concrete crack pattern. As shown, the damage progression was similar to specimen OOPM-C. The first flexural crack occurred at 18% of P_{max}. As the load increased, additional flexural cracks were formed within the RC wall shear span, as well as in the SC wall region around 150 kips (0.26P_{max}). The flexural cracks transformed into flexural-shear cracks, and cracks appeared in the connection region at 52% of P_{max}. After the yielding of the #14 reinforcement, the compression zone under the loading point (RC wall portion) softened as a result of concrete crushing and spalling, which initiated around 90% of P_{max} as shown in Figure 26(a). Thus, the beam deformations became prominent as the specimen deflected in a ductile manner, as shown in Figure 26(b).

NUMERICAL INSIGHT INTO BEHAVIOR

A three-dimensional (3D) finite element model (FEM) was developed and analyzed to provide better insight into the force transfer mechanism for the design demand. Analysis was conducted to predict the performance, strength, ductility, and failure mode of the designed specimens. The tests described in the previous section were simulated using the commercially available finite element modeling (FEM) software LS-DYNA, (LS-DYNA, 2012a, 2012b) employing an explicit time-stepping algorithm.

Analysis Approach

The concrete in the SC and RC wall portions, the SC wall faceplate, and the connection region (wing plates, tie plates, and baseplates), as well as the RC wall flexural reinforcement, were modeled using eight-node hexahedron solid elements with six degrees of freedom per node as shown in Figure 27. The two most common integration techniques used for solid elements in LS-DYNA are the reduced and full integration technique (LS-DYNA, 2012a, 2012b). Concrete was modeled using a computationally less extensive constant stress (ELFORM 1, reduced integration) formulation. However, the connection region, SC wall faceplate, and flexural reinforcement (#14 rebar) were modeled using full integration element formulation due to the nature of their geometries. While the reduced integration technique has an inherent drawback of introducing zero energy modes, commonly referred to as hourglass modes, it does compensate by providing the computational efficiency. The potential hour glassing issue was prevented by introducing stiffness-based hourglass control with an hour-glassing coefficient of 0.1 consistent with the values used by Yang (2015). On the contrary, full integration technique is prone to shear interlocking in case of pure bending. To overcome the issue, the LS-DYNA full integration type for poor aspect ratio (ELFORM 1) was used to reduce transverse shear locking. The Hughes-Liu beam element formulation (ELFORM 1)

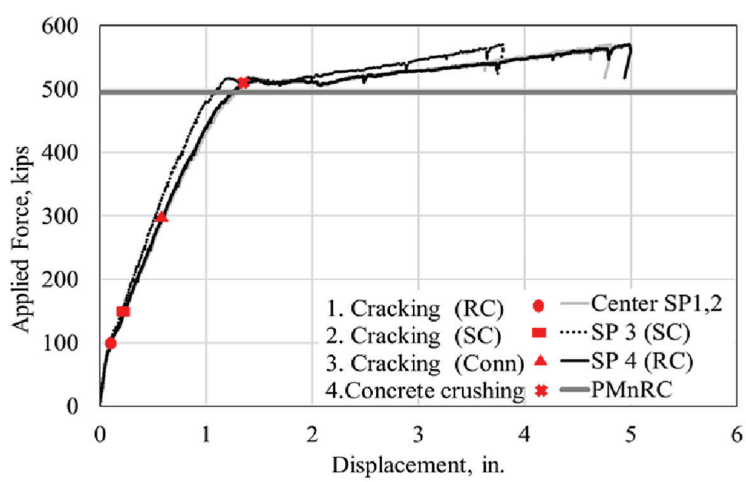

Fig. 23. Applied force–displacement response of specimen OOPM-DN.

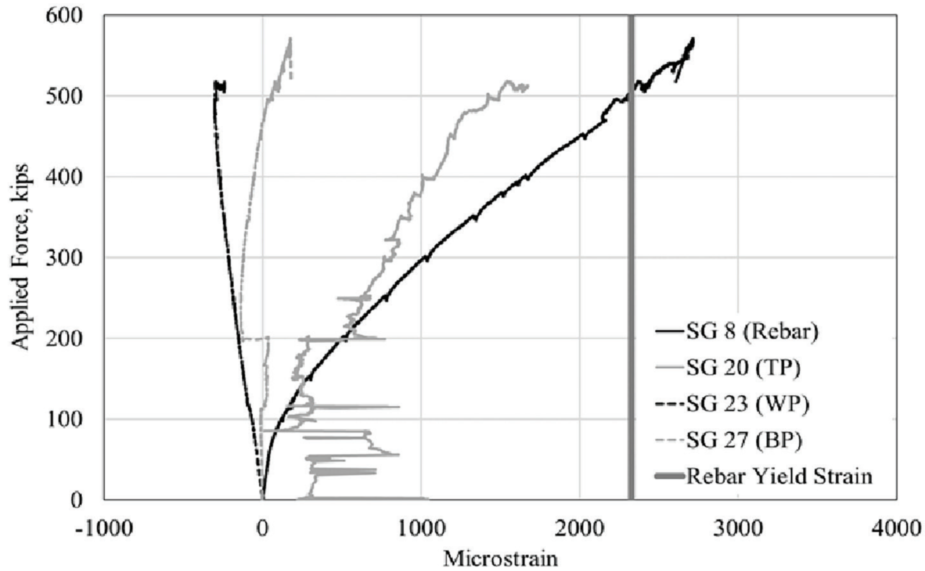

Fig. 24. Applied force–strain response of specimen OOPM-DN (#14 rebars, wing plates, tie plates, and baseplates).

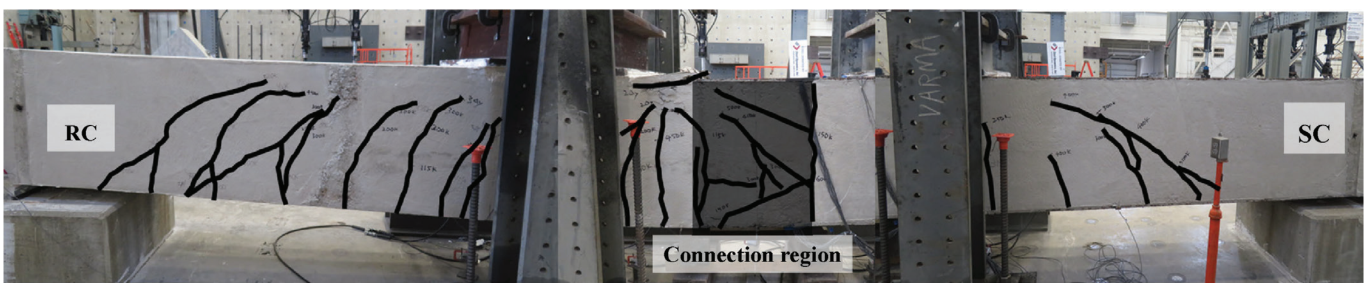

Fig. 25. Concrete crack pattern (east side)—specimen OOPM-DN.

(a) Concrete crushing at the RC loading point

(b) Significantly deformed specimen

Fig. 26. Damage of specimen OOPM-DN.

was used to explicitly model the RC wall shear reinforcement, SC wall shear studs, and tie bars using two node beam elements with one-point integration and a circular cross section, as shown in Figure 28. These element formulations are evaluated by various authors, including Bruhl et al. (2015b) and Epackachi et al. (2015). Both definitions for solid and beam elements are accessible via SECTION_SOLID keyword. The average size of a solid element across the faceplate and the concrete infill is 1 in.

RC wall reinforcement and SC wall studs and tie bars (tied to the faceplate) were embedded in the respective concrete portions by coupling the acceleration and velocity via the Constrained_Lagrange_In_Solid (CLIS) keyword to depict a perfect bond behavior. Connection region tie plates, wing plates, and baseplates were also coupled to the SC wall infill concrete using the same constraint definition. Interaction between SC wall infill concrete and faceplate was defined using the Automatic_Surface_To_Surface formulation. This two-way contact definition prevents the slave and master nodes from penetration. In the tangential direction, a median value of coefficient of friction equal to 0.64, reported by Rabbat and Russel (1985), was used. The embedment length of the RC wall flexural reinforcement extending inside the SC wall was less than the required development length from ACI 349 (ACI, 2006); therefore, it was not embedded inside the SC wall (connection region), and its interaction with infill concrete was also defined using the same contact definition. Additionally, the interaction between loading plates, support rollers, and corresponding surfaces of RC and SC walls were simulated using the same contact formulation.

Material Models and Properties

Continuous_Surface_Cap_Model (CSCM) concrete (MAT 159), chosen from the library of LS-DYNA (LS-DYNA, 2012a, 2012b), is an isotropic model that requires only basic strength data (f_c') and aggregate size. Therefore, it minimizes the need for expansive testing to determine a wide range of parameters. The input compressive strength was based on the average values obtained on the day of tests. The concrete material model (MAT 159) was developed as part of an effort to predict the performance of roadside concrete safety structures. The strength of the isotropic cap model revolves around the smooth intersection between failure and cap surfaces. To simulate concrete damage progression such as cracking, crushing, and spalling, element erosion criteria in the form of maximum and

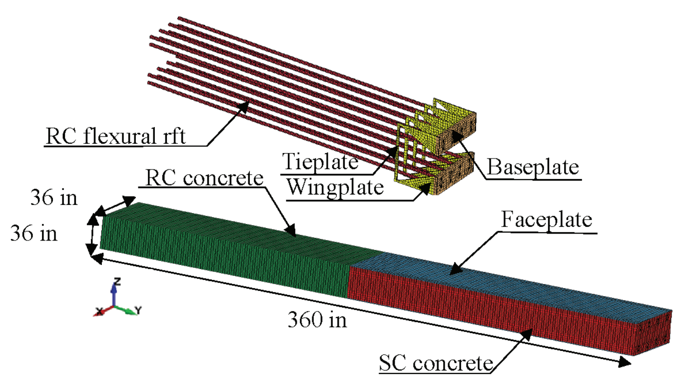

Fig. 27. FEM solid element formulation.

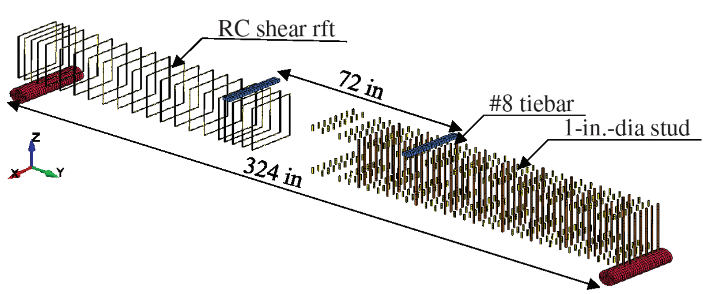

Fig. 28. FEM beam element formulation.

Table 3. Input Parameters for LS-DYNA Material Models			
Material Type	Input Parameters	Value/Equation	Reference
Concrete	Mass density	2.25×10^{-4} lbfs^2/in.	
	Unconfined compression strength	Table 2	Based on material tests
	Maximum aggregate size	0.750 in.	Experimental data
	Erosion criteria: MNEPS MXEPS	 –0.003 0.005	 Equation 6
Steel	Mass density	7.34×10^{-4} lbfs^2/in.	
	Young's modulus	2.90×10^{7} psi	
	Poisson's ratio	0.300	
	Yield strength	Table 2	Based on material tests
	Failure strain	Table 2	Based on material tests
	Stress–plastic strain curve	Table 2	Based on material tests
	Hardening variable	0	LS-DYNA (2012a, 2012b)

minimum principal strains were artificially included by defining a MAT_ADD_EROSION keyword. A concrete ultimate compressive strain value of −0.003 was specified as minimum principal strain (MNEPS), whereas maximum principal strain (MXEPS) was calculated using Equation 6. These values are consistent with the findings obtained by Yang (2015), where ω is the crack width at zero tensile strength and V_e is the volume of one solid element. Concrete crack width, ω, can be estimated from Equation 7. In Equation 7, f_t is uniaxial tensile strength and G_f is specified fracture energy, which can be estimated using Equation 8 (Wittmann et al., 1988). In Equation 8, Φ is the maximum aggregate size.

$$\text{Maximum principal strain (MXEPS)} = \frac{\omega}{\sqrt[3]{V_e}} \tag{6}$$

$$\omega = \frac{2G_f}{f_t} \tag{7}$$

$$G_f = 1.297\Phi^{0.32} \tag{8}$$

RC wall reinforcement, connection region, and SC wall faceplates were modeled using the Piecewise_Linear_Plasticity material model (MAT 24). It is a constitutive steel material model with isotropic elastic, von Mises yield criterion, associated flow rule, and post-yield plastic behavior (Kurt et al., 2016). MAT 24 provides the flexibility of defining post-yield hardening behavior in form of effective stress-plastic strain curves averaged from standard uniaxial tension coupon tests performed during the experimentation phase, thus allowing explicit modeling of nonlinear behavior. SC wall shear studs and tie bars were modeled with Plastic_kinematic (MAT 03) material model. Both the steel models are featured with a strain rate scale effect, which was not activated due to quasi-static nature of tests. Additionally, Rigid material (MAT 20) was used to provide material definition for loading beams and roller supports. Table 3 summarizes the material properties used in the simulations.

Analytical Verification

Figure 29 shows the analytically predicted applied force-displacement response of the model mapped over the experimentally measured response of the OOPM-C test specimen. As shown, the analytically predicted response is in close agreement with the experimentally measured response. The displacement is measured under the RC wall portion loading point (36 in. from the interface of SC wall region). The analytically predicted maximum load, P_{max}^{FEA}, was 571 kips, which is greater than the force associated with the flexural strength of the RC wall portion, $P_{Mn.RC} = 495$ kips, by 15%. The shear force, V_{Pmax}^{FEA}, associated with the analytically predicted P_{max}^{FEA} was 286 kips, which is less than the shear strength of the RC wall portion ($V_{n.RC}$ = 329 kips), confirming flexural yielding as the governing failure mode.

The maximum stress predicted in the bottom layer of #14 rebar was approximately 93 ksi, which is just over 125% of the yield stress of the reinforcing bars ($1.25F_{y,r}$ = 83.3 ksi). Longitudinal strain responses predicted by the model are compared with experimentally measured strain responses in Figure 30. In the case of the tie plate, SG 20 values were compared directly with corresponding simulated strains in Figure 30(a). In Figure 30(b), the same comparison is shown for the wing plate (SG 22). The simulated strain values are in a reasonable agreement compared with observed data in this case. Strain contour plots of the mechanical connection region at P_{max}^{FEA} are shown in Figure 31. As shown, the maximum predicted strain values for the tie plate (corresponding to SG 20) and wing plate (corresponding to SG 22) are somewhat lower than the experimental data. This was attributed to the treatment of the interface between concrete and the steel plates in the connection region in the model. The steel plates (tie plate, wing plate, and baseplate) were embedded in concrete in the model, which allows the perfect composite action. However, no perfect composite action is developed in the connection region of the specimens. Only a limited level of bonding between the steel plates and concrete is achieved. For this reason, the tie plate and wing plate carried lower stress and exhibited lower strain. However, all steel components (including tie plate, wing plate, and baseplate) in the connection region remained in the elastic range until the connected RC wall portion developed its flexural strength (RC flexural yielding), which is in accordance with the experimental observation.

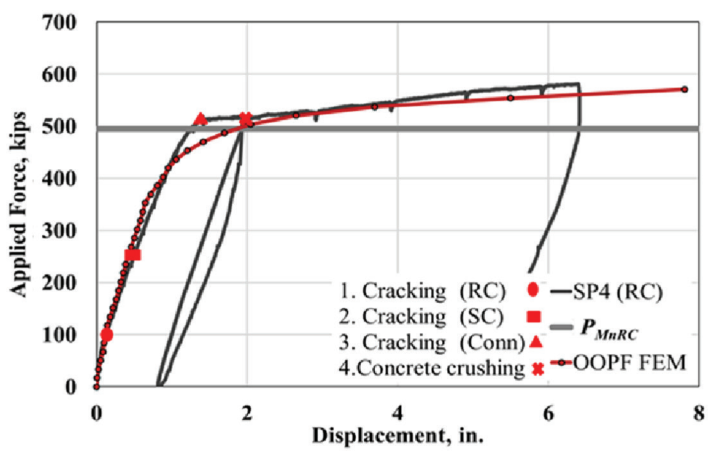

Fig. 29. Comparison between experimental (OOPM-C) and FEA results.

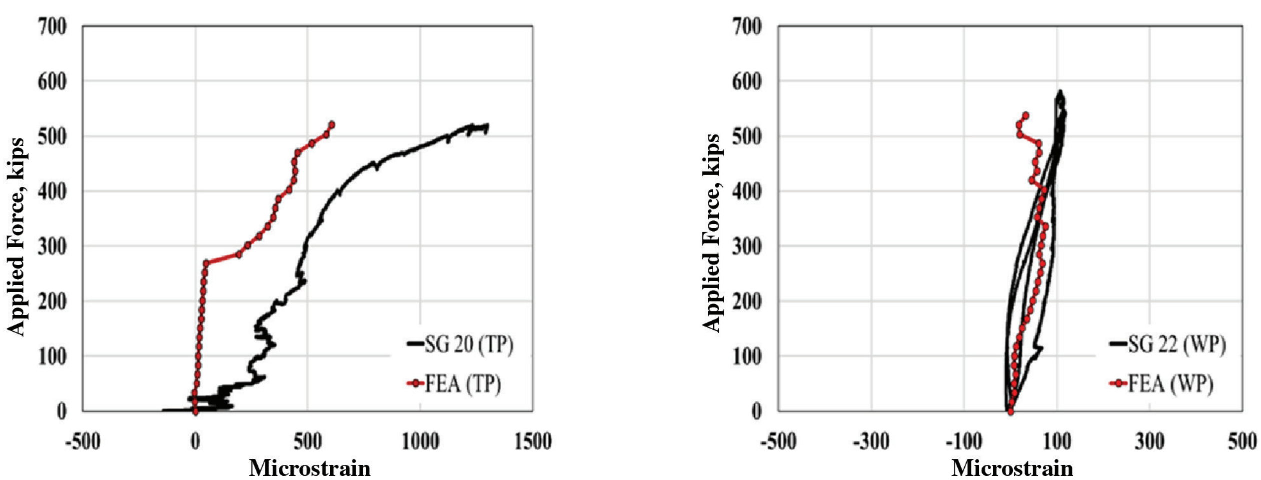

(a) Tie plate

(b) Wing plate

Fig. 30. Strain gauge data (experimental vs. FEA).

SUMMARY AND CONCLUSIONS

Both experimental and numerical investigations were conducted to evaluate the design procedure developed for SC wall-to-RC wall mechanical connections. The design procedure was developed based on the full-strength connection design philosophy. The applied force-displacement responses and the applied force-steel strain responses were measured and evaluated to determine the ultimate strength and the governing failure. The measured strengths were compared with the RC wall strength determined using ACI 349 (ACI, 2006). The results from both experimental and analytical investigations indicated the following:

1. The governing failure mode of the two test specimens was flexural yielding of the RC components, ensuring energy dissipation away from the connection region. Thus, the connection region can be designed and detailed using the proposed design procedure.
2. The type of connection plan, coupler or double nut, had no influence on the force transfer mechanism of the designed connection.
3. The measured ultimate strength was 585 kips for specimen OOPM-C and 571 kips for specimen OOPM-DN, which was greater than the ACI code equation by 18% and 15%, respectively.
4. All the steel components in the connection region remained in the elastic range until the RC wall developed its full flexural strength.
5. The experimentally observed and analytically predicted maximum strain values in the case of the wing plates and baseplates were well under their yield strain, indicating a significant contribution of the concrete in the force transfer mechanism and exhibiting conservatism in the design procedure.
6. The proposed design procedure is suitable and conservative for designing SC wall-to-RC mechanical connections. However, additional experimental and analytical studies should be conducted to expand the limited database and further verify the design procedure for different loading conditions such as in-plane and out-of-plane shear.

ACKNOWLEDGMENTS

This research was funded by KEPCO E&C, Korea, and the specimens were tested at Bowen Laboratory at Purdue University. The authors acknowledge the valuable contributions of the sponsor and all the technical staff involved in the experimental and analytical work throughout the execution of the project. However, the views presented in this paper are solely those of the authors.

REFERENCES

ACI (2006), *Code Requirements for Nuclear Safety-Related Concrete Structures and Commentary*, ACI 349-06, American Concrete Institute, Farmington Hills, Mich.

ACI (2019), *Building Code Requirements for Structural Concrete*, ACI 318–19, American Concrete Institute, Farmington Hills, Mich.

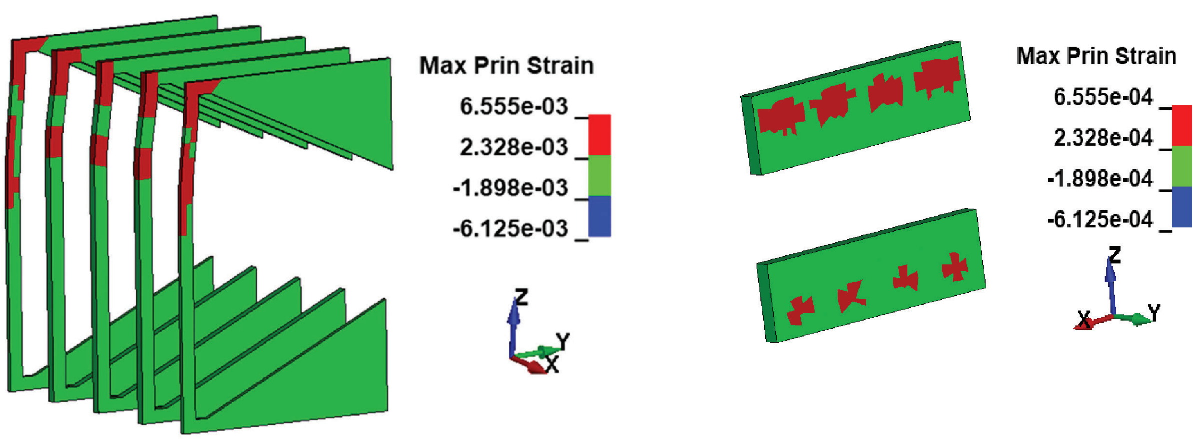

(a) Tie plate and wing plate *(b) Baseplate*

Fig. 31. Strain contour plot.

AISC (2016), *Seismic Provisions for Structural Steel Buildings*, ANSI/AISC 341-16, American Institute of Steel Construction, Chicago, Ill.

AISC (2018), *Specification for Safety-Related Steel Structures for Nuclear Facilities*, ANSI/AISC N690-18, American Institute of Steel Construction, Chicago, Ill.

AISC (2019), *Companion to the AISC Steel Construction Manual, Volume 1: Design Examples*, Version 15.1, American Institute of Steel Construction, Chicago, Ill.

ASTM (2013), *Standard Test Method for Tension Testing of Metallic Materials*, ASTM E8/E8M, ASTM International, West Conshohocken, Pa.

ASTM (2014), *Standard Test Method for Compressive Strength of Cylindrical Concrete Specimens*, ASTM C39/C39M, ASTM International, West Conshohocken, Pa.

ASTM (2016), *Standard Specification for Deformed and Plain Low-Alloy Steel Bars for Concrete Reinforcement*, ASTM A709/A709M-16, ASTM International, West Conshohocken, Pa.

ASTM (2020), *Standard Specification for Hex Cap Screws, Bolts and Studs, Steel, Heat Treated, 120/105/90 ksi Minimum Tensile Strength, General Use*, ASTM A449-14 (2020), ASTM International, West Conshohocken, Pa.

Bhardwaj, S.R., Sener, K.C., and Varma, A.H. (2019), "Multi-Hazard Investigation and Testing of Steel-Plate Composite (SC) Wall Piers: Seismic and Thermal Loads," *Nuclear Engineering and Design*, Vol. 348, pp. 121–130. https://doi.org/10.1016/j.nucengdes.2019.03.026

Bhardwaj, S.R. and Varma, A.H. (2017), *Design of Modular Steel-Plate Composite Walls for Safety Related Nuclear Facilities*, Design Guide 32, AISC, Chicago, Ill.

Bruhl, J.C., Varma, A.H., and Johnson, W.H. (2015a), "Design of Composite SC Walls to Prevent Perforation from Missile Impact," *International Journal of Impact Engineering*, Vol. 75, pp. 75–87. https://doi.org/10.1016/j.ijimpeng.2014.07.015

Bruhl, J.C., Varma, A.H., and Kim, J.M. (2015b), "Static Resistance Function for Steel-Plate Composite (SC) Walls Subject to Impactive Loading," *Nuclear Engineering and Design*, Vol. 295, pp. 843–859. https://doi.10.1016/j.nucengdes.2015.07.037

Choi, B.J. and Han, H.S. (2009), "An Experiment on Compressive Profile of the Unstiffened Steel Plate-Concrete Structures under Compression Loading," *Steel and Composite Structures*, Vol. 9, No. 6, pp. 519–534. https://doi.org/10.12989/scs.2009.9.6.519

Epackachi, S., Whittaker, A.S., Varma, A.H., and Kurt, E.G. (2015), "Finite Element Modeling of Steel-Plate Concrete Composite Wall Piers," *Engineering Structures*, Vol. 100, pp. 369–384.

Foundoukos, N. and Chapman, J.C. (2008), "Finite Element Analysis of Steel–Concrete–Steel Sandwich Beams," *Journal of Constructional Steel Research*, Vol. 64, No. 9, pp. 947–961. https://doi.org/10.1016/j.jcsr.2007.10.011

Hong, S.G., Lee, K.J., Park, D.S., Ham, K.W., and Lee, H.W. (2009), "Out-of-Plane Shear Strength of Steel Plate Concrete Walls Dependent on Bond Behavior," *Proceedings of 20th International Conference on Structural Mechanics in Reactor Technology (SMiRT-20)*, Div-6: Paper ID# 1855, August 9–14, Espoo, Finland.

Hwang, K.M., Lee, K.J., and Kim, W.K. (2013), "An Experimental Study on the Flexural and Shear Behavior of Steel Plate Concrete–Reinforced Concrete Connected Structures," *Nuclear Engineering and Design*, Vol. 257, pp. 88–99. https://dx.doi.org/10.1016/j.nucengdes.2012.12.020

JEAC (2009), *Technical Code for Seismic Design of Steel Plate Reinforced Concrete Structures: Buildings and Structures*, JEAC-4618, Japanese Electric Association Nuclear Standards Committee, Tokyo, Japan.

KEA (2010), *Specification for Safety-Related Steel Plate Concrete Structures for Nuclear Facilities*, KEPIC-SNG, Board of KEPIC Policy, Structural Committee, Korea Electric Association.

Kim, K., Lee, K., Shun, J., Lee, J., and Varma, A.H. (2020), "A Study on the Resistance of SC Walls Subjected to Missile Impact Using Large-Scale Impact Tests," *International Journal of Impact Engineering*, Vol. 139. https://doi.org/10.1016/j.ijimpeng.2020.103507

Kurt, E.G. (2016), "Steel-Plate Composite (SC) Walls and Their Basemat Connections: Seismic Behavior, Analysis, and Design," PhD Dissertation, Purdue University, West Lafayette, Ind.

Kurt, E.G., Varma, A.H., Booth, P., and Whittaker, A.S. (2016), "In-Plane Behavior and Design of Rectangular SC Wall Piers without Boundary Elements," *Journal of Structural Engineering*, Vol. 142, No. 6. https://doi.org/10.1061/(ASCE)st.1943-541x.0001481

Lee, K.J., Hwang, K.M., Hahm, K.W., and Kim, W.B. (2012), "An Experimental Study on Flexural/Shear Load Properties of SC (Steel Plate Concrete) Structure with Reinforced Concrete Joint," *Journal of Korean Society of Steel Construction*, Vol. 24, No. 2. https://doi.org/10.7781/kjoss.2012.24.2.137

Lee, S.J., Choi, B.J., and Kim, T.K. (2009), "An Experimental Study on the Behavior of Steel Plate-Concrete Wall with Vertical Ribs," *Journal of Korean Society of Steel Construction*, Vol. 1, No. 3, pp. 277–287.

Leng, Y.B., Song, X.B., Chu, M., and Ge, H.H. (2015), "Experimental Study and Theoretical Analysis of Resistance of Steel-Concrete-Steel Sandwich Beams," *Journal of Structural Engineering*, Vol. 141, No. 2.

LS-DYNA (2012a), *Keyword User's Manual*, Vol. I, Version 971 R6.0.0, Livermore Software Technology Corporation (LSTC), Livermore, Calif.

LS-DYNA (2012b), *Keyword User's Manual*, Vol. II, Version 971 R6.0.0, Livermore Software Technology Corporation (LSTC), Livermore, Calif.

McKinley, B. and Boswell, L.F. (2002), "Behavior of Double Skin Composite Construction," *Journal of Constructional Steel Research*, Vol. 58, No. 10, pp. 1347–1359. https://doi.org/10.1016/s0143-974x(02)00015-9

Ozaki, M., Akita, S., Osuga, H., Nakayama, T., and Adachi, N. (2004), "Study on Steel Plate Reinforced Concrete Panels Subjected to Cyclic In-Plane Shear," *Nuclear Engineering and Design*, Vol. 228, pp. 225–244. https://doi.org/10.1016/j.nucengdes.2003.06.010

Rabbat, B.G. and Russell, H.G. (1985), "Friction Coefficient of Steel on Concrete or Grout," *Journal of Structural Engineering*, Vol. 111, No. 3, pp. 505–515. https://doi.org/10.1061/(ASCE)0733-9445(1985)111:3(505)

Sener, K.C., Varma, A.H., and Ayhan, D. (2015), "Steel-Plate Composite (SC) Walls: Out-of-Plane Flexural Behavior, Database, and Design," *Journal of Constructional Steel Research*, Vol. 108, pp. 45–59. https://doi.org/10.1016/j.jcsr.2015.02.002

Seo, J. and Varma, A.H. (2017a), "Experimental Behavior and Design of Steel Plate Composite-to-Reinforced Concrete Lap Splice Connections," *Journal of Structural Engineering*, Vol. 143, No. 5. https://doi.org/10.1061/(ASCE)st.1943-541x.0001711

Seo, J. and Varma, A.H. (2017b), "Behavior and Design of Steel-Plate Composite Wall-to-Wall Corner or L-Joints," *Nuclear Engineering and Design*, Vol. 323, pp. 317–328. https://doi.org/10.1016/j.nucengdes.2017.04.008

Seo, J. and Varma, A.H. (2017c), "SC Wall-to-Slab Connections in Safety Related Nuclear Facilities," *Proceedings of 24th International Conference on Structural Mechanics in Reactor Technology (SMiRT-24)*, August 20–25, Busan, Korea.

Seo, J, and Varma, A.H. (2019), "Steel Plate Composite Wall-to-Wall T-Joints: Joint Shear Strength," *Journal of Structural Engineering*, Vol. 145, No. 7. https://doi.org/10.1061/(ASCE)st.1943-541x.0002317

Song, X., Chu, M., Ge, H., and Wang, H. (2014), "A Failure Criterion for Steel-Concrete Composite Walls," *Proceedings of the International Conference on Sustainable Development of Critical Infrastructure*, Shanghai, China. https://doi.org/10.1061/9780784413470.034

Takeuchi, M., Narikawa, M., Matsuo, I., Hara, K., and Usami, S. (1998), "Study on a Concrete Filled Structure for Nuclear Power Plants," *Nuclear Engineering and Design*, Vol. 179, pp. 209–223.

Wittmann, F.H., Rokugo, K., Bruhwiler, E., Mihashi, H., and Simonin, P. (1988), "Fracture Energy and Strain Softening of Concrete as Determined by Means of Compact Tension Specimens," *Materials and Structures*, Vol. 21, No. 121, pp. 21–32.

Yang, Y. (2015), "Shear Strength and Behavior of Reinforced Concrete Structures with T-Headed Bars in Safety-Related Nuclear Facilities," PhD Dissertation, Purdue University, West Lafayette, Ind.

Zhang, K., Seo, J., and Varma, A.H. (2020), "Steel-Plate Composite Walls: Local Buckling and Design for Axial Compression," *Journal of Structural Engineering*, Vol. 146, No. 4. https://doi.org/10.1061/(ASCE)st.1943-541x.0002545